

β -DECAY PROPERTIES OF WAITING-POINT NUCLEI FOR ASTROPHYSICAL APPLICATIONS

JAMEEL-UN NABI, ASIM ULLAH, SYED AHSAN ALI SHAH
GUL DARAZ, MUNIR AHMAD

Faculty of Engineering Sciences
GIK Institute of Engineering Sciences and Technology
Topi 23640, Khyber Pakhtunkhwa, Pakistan

(Received November 19, 2018; accepted October 2, 2019)

We report microscopic calculation of key β -decay properties for some of the crucial waiting-point species having neutron closed magic shells 50 and 82. Our calculation bears astrophysical significance vis-à-vis speeding of the r-process. The β -decay properties include electron emission weak rates, half-lives, energy rates of β -delayed neutrons and their emission probabilities, both under terrestrial and stellar conditions. We perform a *pn*-QRPA calculation with a separable multi-shell interaction and include both allowed and unique first-forbidden transitions in our calculation. We compare our results with previous calculations and measured data. Our calculation is in good agreement with the experimental data. For certain cases, we noted a significant decrease in the half-life calculation once the contribution of unique first-forbidden transitions was added. Our results are not in agreement with the shell model study where only for $N = 126$ waiting-point nuclei the forbidden transitions were reported to significantly reduce the calculated half-lives. Our model fulfills the Ikeda sum rule for even-even cases. For odd- A cases, the rule is violated by up to 0.7% for ^{81}Ga .

DOI:10.5506/APhysPolB.50.1523

1. Introduction

Since the seminal paper on synthesis of elements in stars [1], our understanding of the nucleosynthesis process has greatly improved (for recent references, see *e.g.* [2, 3]). The r- and s-processes are the key phenomena responsible for nucleosynthesis of heavy elements. The r-process mechanism basically requires the understanding of nuclear characteristics of hundreds of neutron-rich nuclide, mostly unknown. The weak interaction rates and reaction cross sections are amongst the key nuclear input data to affect the r-process calculation. The β -decay rates deserve a special mention as they

are responsible for changing the nuclear specie during heavy element synthesis. At the same time, r-process mechanism demands also accurate estimate of other physical parameters including entropy, temperature, density and lepton-to-baryon ratio of the stellar matter. The physical conditions conducive for occurrence of r-process are relatively high temperatures (of the order of few GK) and high neutron densities ($> 10^{20} \text{ cm}^{-3}$) [1, 4–7]. Under prevailing conditions, the capturing process of neutrons takes place at a faster pace than the competing β -decay processes and many neutron-rich nuclei (with $S_n \leq 3 \text{ MeV}$) are produced. Nuclei possessing closed neutron shells of 50, 82 and 126 exhibit discontinuities in neutron separation energies because of a stronger binding energy. Consequently, the r-process matter flow decelerates and waits for occurrence of several β -decays to occur before the process of rapid neutron capture resumes. Peaks have been observed in the distribution abundances of r-mechanism at $N = 50, 82$ and 126 because of accumulation of matter at these waiting-point nuclei. The calculated half-lives of β -decay for waiting-point nuclei describe the time scale it takes the mass flow to transpose seed nuclei to larger nuclei in the third peak at around $A \sim 200$. Provided that the r-mechanism has enough duration time for β -flow equilibrium to built, the β -decay half-lives are proportional to the relative elemental abundances [8].

Unfortunately, the experimental information for waiting-point nuclei is scarce. For the neutron closed shells of $N = 50$ and 82 waiting-point nuclei, the available half-lives are rather limited and insufficient [9–12]. The scenario is expected to improve in the near future with radioactive ion beam experiments at RIKEN [13] and GSI [14]. Hence for r-process simulations, the required β -decay half-lives come primarily from theoretical estimations. An extensive tabulation of microscopic β -decay rates for a wide range of nuclei was reported by Klapdor-Kleingrothaus *et al.* [15]. Later, Staudt *et al.* [16, 17] and Hirsh *et al.* [18] used the proton–neutron quasiparticle random phase approximation (*pn*-QRPA) model, for the first time, to predict β -decay half-lives for a wide range of proton-rich and neutron-rich exotic nuclei. The r-process spectra of waiting-point nuclei can be affected by the presence of low-lying energy levels possessing different parities. This necessitates the incorporation of the first-forbidden (FF) chapter to the β -decay half-lives. The *pn*-QRPA model was used to estimate the FF contributions for a handful of nuclei for the first time by Homma *et al.* [19]. Later, other models were used to estimate the FF contribution. These include, but are not limited to, the QRPA + gross theory [20], self-consistent density-functional + continuum QRPA [21] and, more recently, the large-scale shell model calculation [22]. Only a small percent of the total $3(N - Z)$ sum rule lie within the Q_β window for the neutron-rich nuclei participating in the r-process. The rest of the strength resides in the Gamow–Teller (GT)

giant resonance located at much larger excitation energies. This may furnish explanation as to why different model calculations of β-decay half-lives may differ significantly without violating the sum rule.

Taking the weak-interaction rates to stellar domain is a next level calculation. Nabi and Klapdor-Kleingrothaus used the *pn*-QRPA approach and calculated stellar weak rates of *sd*-, *fp*- and *fp**g*-shell nuclei [23–25] for various astrophysical applications. The current *pn*-QRPA approach, using a separable interaction with a multi- $\hbar\omega$ space, makes possible a state-by-state calculation of weak interaction rates summing over Boltzmann-weighted, microscopically estimated GT strengths for all parent excited levels. This distinguishing feature of current calculation makes it unique amongst all calculations of stellar weak rates (including those using the independent particle model and shell model).

In the present work, we report on the GT strength distribution, half-life, stellar β-decay and positron emission rate, energy rates of β-delayed neutron and corresponding neutron emission probabilities (P_n) calculations for nuclei having neutron magic numbers ($N = 50$ and 82) using the *pn*-QRPA model. Thirteen waiting-point nuclei (six having $N = 50$ and seven having $N = 82$) were selected for this paper. In all cases, we consider both the allowed GT and unique first-forbidden (U1F) transition contribution to the total weak rates. Non-unique transitions are also important. Currently, we are working on codes to calculate non-unique contributions and their inclusion would be taken as a future assignment. We organize our paper in four sections. Section 2 describes the necessary *pn*-QRPA formalism. In Section 3, we show our results and present comparison with measurement and previous calculations. Conclusions and our key findings are stated in Section 4.

2. Theoretical formalism

The addition of all transition probabilities to levels in the daughter state j with energies E_j lying within the Q_β window gives the terrestrial half-life of β-decay

$$T_{1/2} = \left(\sum_{0 \leq E_j \leq Q_\beta} 1/t_j \right)^{-1}, \tag{1}$$

where t_j shows the partial half-life for the allowed β-decay transition given by

$$f_0(Z, Q_\beta - E_j) t_j = \frac{D}{B_F(E_j) + (g_A/g_V)^2 B_{GT}(E_j)}. \tag{2}$$

Here, (g_A/g_V) is axial to vector coupling constant ratio (numerical value is -1.254), D is a physical constant given by $D = 2\pi^3 \hbar^7 \ln 2 / g_V^2 m_e^5 c^4$ (numerical value is 6295 s) and f_0 is the Fermi integral function (taking into

account finite size effects and screening of nucleus, using the recipe of Gove and Martin [26]). The $B_F(E_j)$ and $B_{GT}(E_j)$ gives the reduced transition probabilities of Fermi and GT transitions, respectively. Our model includes GT force with separable particle-hole (ph) and particle-particle (pp) matrix elements. The two forces were characterized by strength parameter χ_{GT} and κ_{GT} , respectively. For the pn -QRPA Hamiltonian, its model parameters, and calculation of reduced transition probabilities, we refer to [17, 18]. The formalism is not repeated here for space consideration.

For the U1F transitions, the pp and ph matrix elements are given by

$$V_{pn,p'n'}^{ph} = +2\chi_{U1F} f_{pn}(\mu) f_{p'n'}(\mu), \quad (3)$$

$$V_{pn,p'n'}^{pp} = -2\kappa_{U1F} f_{pn}(\mu) f_{p'n'}(\mu), \quad (4)$$

where

$$f_{pn}(\mu) = \langle p | t_{-r}[\sigma Y_1]_{2\mu} | n \rangle \quad (5)$$

is a single particle transition amplitude between Nilsson single particle states (deformed). Here, μ values are labeled $\mu = 0, \pm 1$ and ± 2 (which represents the spherical component of the transition operator). Other symbols have regular meaning. The neutron and proton states possess different parities [19].

The role of pp and ph strength interaction constants was discussed in length in previous calculations of β -decay (*e.g.* [17–19]). It is argued that the particle-particle interaction allows one to improve the theoretical β^+ -decay rates and worsen the description of β^- -decay rates. Accordingly, we decided to switch-off the particle-particle interaction in the current calculation. Further, the ph strength interaction constant was chosen as in the earlier pn -QRPA β^- -decay rate calculation [17]. The deformation parameter was taken from [27], while Q -values were taken from [28].

The stellar β -decay rates for allowed GT and U1F transitions from parent (i^{th} level) to daughter (j^{th} level) nucleus were determined using

$$\lambda_{ij}^\beta = \frac{m_e^5 c^4}{2\pi^3 \hbar^7} \sum_{\Delta J^\pi} g^2 f_{ij}(\Delta J^\pi) B_{ij}(\Delta J^\pi). \quad (6)$$

In the above equation $B_{ij}(\Delta J^\pi)$ and $f_{ij}(\Delta J^\pi)$ are the reduced transition probabilities and phase-space factors, respectively. For allowed transitions, the reduced GT ($\Delta J^\pi = 1^+$) transition probabilities are given by

$$B(\text{GT})_{ij} = \frac{1}{2J_i + 1} \left| \langle j \parallel \sum_k t_-^k \vec{\sigma}^k \parallel i \rangle \right|^2. \quad (7)$$

The reduced Fermi ($\Delta J^\pi = 0^+$) transition probabilities are given by

$$B(\text{F})_{ij} = \frac{1}{2J_i + 1} \left| \langle j \parallel \sum_k t_-^k \parallel i \rangle \right|^2. \quad (8)$$

The phase-space integral (f_{ij}) is an integral over total energy. For the case of β -decay, it is given by (from here onwards we use natural units, $\hbar = m_e = c = 1$)

$$f_{ij} = \int_1^{w_m} w \sqrt{w^2 - 1} (w_m - w)^2 F(+Z, w) (1 - G_-) dw, \tag{9}$$

whereas for continuum positron capture, phase space is given by

$$f_{ij} = \int_{w_l}^{\infty} w \sqrt{w^2 - 1} (w_m + w)^2 F(-Z, w) G_+ dw. \tag{10}$$

For the U1F transitions,

$$B_{ij}(\Delta J^\pi) = \frac{1}{12} z^2 (w_m^2 - 1) - \frac{1}{6} z^2 w_m w + \frac{1}{6} z^2 w^2, \tag{11}$$

where z is

$$z = 2g_A \frac{\langle j \parallel \sum_k r_k [\mathbf{C}_1^k \times \sigma]^2 \mathbf{t}_-^k \parallel i \rangle}{\sqrt{2J_i + 1}}, \tag{12}$$

$$\mathbf{C}_{lm} = \sqrt{\frac{4\pi}{2l + 1}} \mathbf{Y}_{lm}, \tag{13}$$

\mathbf{Y}_{lm} are the spherical harmonics. In the case of U1F interaction, f_{ij} (phase-space integral) were calculated using

$$f_{ij} = \int_1^{w_m} w \sqrt{w^2 - 1} (w_m - w)^2 [(w_m - w)^2 F_1(Z, w) + (w^2 - 1) F_2(Z, w)] (1 - G_-) dw, \tag{14}$$

where the upper limit of the integral gives the total β -decay energy given by ($w_m = m_p - m_d + E_i - E_j$). w is the total energy of the electron including its rest mass. One should note that if the corresponding electron emission total energy, w_m , is greater than -1 , then $w_l = 1$, and if it is less than or equal to 1 , then $w_l = |w_m|$. The G_+ and G_- are the positron and electron distribution functions, respectively. The $F(\pm Z, w)$, $F_1(Z, w)$ and $F_2(Z, w)$ are the Fermi functions computed using the recipe of [26].

The high temperature inside the core of massive stars signifies that there is a finite probability of occupancy of parent excited levels in stellar scenario. Using the assumption of thermal equilibrium, the occupation probability of i^{th} state can be computed using

$$P_i = \frac{\exp(-E_i/kT)}{\sum_{i=1} \exp(-E_i/kT)}. \quad (15)$$

Finally, the stellar β -decay rate per unit time per nucleus was determined using

$$\lambda^\beta = \sum_{ij} P_i \lambda_{ij}^\beta. \quad (16)$$

A similar sum was performed to calculate continuum positron capture rates in stellar matter. Summations were carried out for all initial states as well as for final states until desired convergence was obtained in our rate calculation. In our calculation, it was further assumed that all daughter excited states having energy larger than the neutron separation energy (S_n) decayed by neutron emission. The energy rate for neutron emission from daughter system was determined using

$$\lambda^n = \sum_{ij} P_i \lambda_{ij}(E_j - S_n), \quad (17)$$

for all $E_j > S_n$. The probability of β -delayed neutron emission, P_n , was calculated using

$$P_n = \frac{\sum_{ij'} P_i \lambda_{ij'}}{\sum_{ij} P_i \lambda_{ij}}, \quad (18)$$

where j' indicates the energy levels of the daughter nucleus with $E_{j'} > S_n$. The $\lambda_{ij(i)}$ in Eq. (17) and Eq. (18) represents the sum of positron capture and electron emission rates, for transition arising from $i \rightarrow j(j')$.

3. Results and discussions

In this section, we are going to present the terrestrial β -decay half-lives, stellar weak rates, phase space and charge-changing strength distribution calculations, including both allowed GT and U1F transitions. The predictive power of the pn -QRPA model becomes more effective for smaller $T_{1/2}$ values (with increasing distance from the stability line) [18, 29] which justifies the usage of present model for β -decay calculations. We compare our calculation with several previous pioneering calculations [20–22, 30, 31] as well as with experimental data [28]. It is to be noted that no quenching factor was used in our calculation. We computed the terrestrial electron emission half-lives

for isotopic chain of neutron rich Cu isotopes presented in [32]. In the present project, we are targeting some astrophysically crucial closed shell nuclei composed of $N = 50$ and 82 . Of interest would be weak rates for a larger number of nuclei around closed neutron shells, as the few examples provided here do not allow a complete assessment. We plan to investigate more heavy nuclei of $N = 126$ (simulations of weak rates are too time consuming especially for heavy mass nuclei) in the near future, expecting some interesting results by employing the same deformed pn -QRPA model.

The allowed GT and U1F electron emission rates for selected $N = 50$ and 82 isotopes are shown in Table I and Table II, respectively.

The rates are shown at different stellar temperatures in units of 10^9 K at stellar densities of $\rho Y_e = 10^3$, $\rho Y_e = 10^7$ and $\rho Y_e = 10^{11}$ (calculated in units of g cm^{-3}) corresponding to low, intermediate and high stellar densities, respectively. The weak rates are tabulated in logarithmic (to base 10) scale in units of s^{-1} . It is to be noted that we have calculated the weak interaction rates for a wide range of temperature from $T_9 = 0.01$ K to $T_9 = 30$ K (where T_9 gives core temperature in units of GK), including the typical r-process temperature domain ranging between $T_9 = (1-3)$ K. The results shown in rate tables depict that electron emission rates increase with rise in temperature due to the contribution of excited state partial rates. The electron emission rates decrease substantially by order of magnitude due to stiffening of stellar core at high density. At high stellar density, the available phase space for electrons reduces due to the Pauli blocking.

The computed β -decay terrestrial half-lives for r-process waiting-point nuclei having $N = 50$ and 82 , including allowed GT and U1F contributions, are shown in Table III. Here, we also show the shell model calculations [33, 34] with only allowed GT contribution, the large scale shell model (LSSM) calculation [22] including both allowed GT and first-forbidden (FF) contributions, and the QRPA calculation performed by [20] where the allowed GT part was calculated using the QRPA model and gross theory was employed to calculate the FF contribution. Experimental half-lives were taken from the recent atomic mass data evaluation of [28]. The LSSM calculation consists of FF transition rates with rank 0, 1 and 2 operator values. It was concluded in the LSSM study that for nuclei having proton number greater or equal to twenty eight and neutron number equal to fifty, the contribution of U1F (rank 2) rates were significant to the FF rates. For ^{79}Cu , the deformed pn -QRPA and LSSM calculated half-life values deviate approximately by 2% and 12%, respectively, from the experimental data [28]. There are three main differences between LSSM and deformed pn -QRPA calculations. In the current pn -QRPA model calculation, we are not able to calculate the rank 0 and 1 operator rates, performed earlier by LSSM. In the LSSM calculation different quenching values ranging from 0.38 to 1.266

TABLE I

Calculated allowed and unique first-forbidden (U1F) electron emission rates of $N = 50$ isotopes for different selected densities and temperatures in stellar matter. ρY_e shows the stellar densities in units of g cm^{-3} , whereas T_9 the stellar temperature in units of 10^9 K. The calculated emission rates are tabulated in logarithmic (to base 10) scale in units of s^{-1} .

Nuclei	T_9 [K]	λ^β [s^{-1}] (allowed)			λ^β [s^{-1}] (U1F)		
		$\rho Y_e = 10^3$	$\rho Y_e = 10^7$	$\rho Y_e = 10^{11}$	$\rho Y_e = 10^3$	$\rho Y_e = 10^7$	$\rho Y_e = 10^{11}$
^{76}Fe	1	-0.58	-0.60	-80.27	1.65	1.65	-89.18
	3	-0.58	-0.60	-27.91	1.65	1.65	-29.91
	5	-0.57	-0.59	-16.94	1.65	1.65	-17.66
	10	-0.19	-0.20	-8.17	1.70	1.70	-8.12
	30	0.89	0.89	-1.70	2.35	2.35	-0.75
^{77}Co	1	1.91	1.91	-44.13	1.97	1.97	-68.08
	3	2.07	2.06	-16.17	2.13	2.14	-22.88
	5	2.11	2.10	-10.09	2.18	2.18	-13.43
	10	2.18	2.18	-4.64	2.29	2.29	-5.91
	30	3.09	3.09	0.62	3.16	3.16	0.46
^{78}Ni	1	-0.02	-0.05	-73.67	0.79	0.78	-85.41
	3	-0.02	-0.05	-25.10	0.79	0.78	-29.57
	5	-0.02	-0.04	-14.97	0.79	0.78	-17.90
	10	0.35	0.35	-6.81	0.85	0.85	-8.74
	30	2.00	2.01	-0.46	1.69	1.69	-1.38
^{79}Cu	1	1.70	1.69	-65.15	0.13	0.12	-97.76
	3	1.73	1.72	-23.07	0.21	0.19	-33.37
	5	1.73	1.73	-14.20	0.29	0.28	-20.14
	10	1.77	1.77	-6.81	0.44	0.43	-9.89
	30	2.84	2.84	-0.04	1.39	1.39	-1.83
^{80}Zn	1	0.29	0.22	-85.05	-0.23	-0.26	-97.48
	3	0.29	0.21	-28.78	-0.23	-0.26	-33.83
	5	0.28	0.25	-17.08	-0.24	-0.26	-20.76
	10	0.64	0.63	-7.59	-0.15	-0.16	-10.56
	30	2.20	2.19	-0.49	0.67	0.67	-2.58
^{81}Ga	1	0.61	0.57	-78.54	-0.29	-0.39	-100
	3	0.59	0.55	-27.51	-0.16	-0.23	-35.54
	5	0.60	0.57	-16.83	-0.11	-0.15	-21.56
	10	0.94	0.93	-7.96	0.09	0.08	-10.65
	30	2.61	2.61	-0.27	1.16	1.16	-2.16

TABLE II

The same as Table I, but for $N = 82$ waiting points.

Nuclei	T_9 [K]	λ^β [s ⁻¹] (allowed)			λ^β [s ⁻¹] (UIF)		
		$\rho Y_e = 10^3$	$\rho Y_e = 10^7$	$\rho Y_e = 10^{11}$	$\rho Y_e = 10^3$	$\rho Y_e = 10^7$	$\rho Y_e = 10^{11}$
¹²⁵ Tc	1	1.56	1.56	-47.61	2.29	2.29	-65.35
	3	1.55	1.55	-17.38	2.64	2.64	-21.42
	5	1.58	1.58	-10.48	2.79	2.79	-12.22
	10	1.93	1.93	-3.88	2.93	2.93	-4.97
	30	3.68	3.68	1.56	2.91	2.91	0.27
¹²⁶ Ru	1	1.01	1.00	-66.09	1.20	-69.28	-69.28
	3	1.01	1.01	-22.35	1.22	-21.76	-21.76
	5	1.03	1.03	-12.94	1.95	-11.85	-11.84
	10	1.47	1.47	-5.39	3.35	-3.99	-3.99
	30	2.54	2.54	0.07	3.98	1.49	1.48
¹²⁷ Rh	1	1.87	1.87	-57.50	0.46	0.45	-76.48
	3	1.84	1.83	-20.24	1.24	1.24	-25.53
	5	1.82	1.81	-11.75	1.58	1.58	-14.96
	10	2.14	2.14	-4.16	1.86	1.86	-6.73
	30	3.91	3.91	1.73	1.90	1.90	-0.91
¹²⁸ Pd	1	0.72	0.71	-73.89	0.80	0.79	-93.84
	3	0.72	0.71	-24.87	0.80	0.79	-31.95
	5	0.74	0.74	-14.35	0.80	0.79	-19.24
	10	1.33	1.33	-6.00	0.85	0.84	-9.39
	30	2.48	2.48	-0.04	0.95	0.95	-2.31
¹²⁹ Ag	1	1.84	1.83	-65.74	-0.11	-0.15	-85.62
	3	1.82	1.81	-22.88	0.49	0.49	-28.69
	5	1.77	1.77	-13.17	0.98	0.97	-16.93
	10	2.08	2.08	-4.72	1.41	1.40	-7.79
	30	3.88	3.88	1.65	1.58	1.57	-1.38
¹³⁰ Cd	1	1.19	1.16	-83.58	0.55	0.54	-89.79
	3	1.19	1.16	-27.44	0.55	0.54	-30.67
	5	1.20	1.16	-15.44	0.55	0.54	-18.54
	10	1.87	1.86	-6.04	0.56	0.55	-9.17
	30	3.24	3.24	-0.6	0.83	0.83	-2.26
¹³¹ In	1	1.58	1.58	-77.14	-1.44	-1.57	-100
	3	1.58	1.57	-26.63	-0.84	-0.87	-33.88
	5	1.64	1.53	-15.55	-0.20	-0.21	-20.26
	10	1.77	1.77	-5.80	0.41	0.41	-9.72
	30	3.78	3.78	1.42	0.65	0.65	-2.53

were used, whereas the deformed pn -QRPA approach (this work) did not incorporate any quenching factor as mentioned earlier. Last but not least, authors in Ref. [22] were not able to recover the full GT and first-forbidden strengths built on the ground and isomeric states due to a model space limitation. A completely converged calculation of the FF transition strength was not possible in the LSSM calculation due to computational limitations. The LSSM calculation used a Lanczos scheme with 100 iterations which was able to converge the states for excitation energies in the vicinity of only 2.5 MeV. The deformed pn -QRPA model, employed in the current calculation, has no such computational limitations and convergence was achieved for excitation energies well in excess of 10 MeV. It may be noted from Table III that the pn -QRPA calculated half-lives are in very good agreement with measured half-lives. The U1F contribution in the current deformed pn -QRPA model is well within the percentage contribution of first-forbidden transitions (to the total half-lives) as calculated by authors in Ref. [20].

TABLE III

Comparison of our computed β -decay half-lives (in units of seconds) for $N = 50$ and 82 r-process waiting-point nuclei with previous calculations and experimental half-lives. Half-lives mentioned with an asterisk in the last column were adopted from [20].

Nuclei	A	SM [33, 34]	LSSM [22]	QRPA+		This work		Exp. [28]
		$T_{1/2}$ (GT)	$T_{1/2}$ (GT+FF)	$T_{1/2}$ (GT)	$T_{1/2}$ (GT+FF)	$T_{1/2}$ (GT)	$T_{1/2}$ (GT+U1F)	
Fe	76	0.008	0.008	0.045	0.027	0.060	0.012	0.013*
Co	77	0.016	0.016	0.013	0.014	0.025	0.016	0.015
Ni	78	0.127	0.150	0.477	0.224	1.210	0.102	0.122
Cu	79	0.222	0.270	0.430	0.157	0.436	0.235	0.241
Zn	80	0.432	0.530	3.068	1.260	0.851	0.557	0.562
Ga	81	0.577	1.030	1.568	1.227	3.387	1.083	1.217
Tc	125	0.009	0.010	0.009	0.009	0.017	0.008	0.008*
Ru	126	0.020	0.020	0.034	0.030	0.027	0.017	0.017*
Rh	127	0.028	0.028	0.022	0.020	0.032	0.029	0.028
Pd	128	0.046	0.047	0.125	0.074	0.042	0.035	0.035
Ag	129	0.070	0.070	0.047	0.032	0.052	0.049	0.050
Cd	130	0.162	0.164	1.123	0.502	0.135	0.122	0.127
In	131	0.260	0.248	0.147	0.139	0.286	0.281	0.261

Table IV shows a similar comparison of our calculated *β*-decay half-lives of *N* = 50 r-process waiting-point nuclei with previous QRPA calculations and measured data. Here, we compare with the self-consistent density-functional and continuum QRPA framework including the GT and FF transitions calculation [21], a QRPA calculation using finite-range droplet model (FRDM), folded-Yukawa single particle potential [31], and the QRPA calculations by [30]. For details of KHF, QRPA-1 and QRPA-2 calculations, we refer to [30]. In the FRDM+RPA calculation [31], odd–even effects were prominent in the *β*-decay half-life values due to the exclusion of the useful *pn*-interaction in particle–particle (*pp*) channel. Borzov [21] used the (DF3 +CQRPA) model for the calculation of allowed and U1F charge-changing transitions, and considered only spherical nuclei. Later, Hosmer [35] pointed out that the spherical shape assumption in Borzov study was not desirable and deformation of the nuclide can have a considerable effect on the *β*-decay half-lives. Only allowed GT rates were computed in the QRPA calculation of [30]. The comparison of current computation with measured data is far better than previous calculations.

TABLE IV

Comparison of our computed *β*-decay half-lives (in units of seconds) for *N* = 50 r-process waiting-point nuclei with previous calculations and experimental half-lives [28].

		Exp.	Borzov [21]	Möller [31]	Pfeiffer <i>et al.</i> [30]			This work	
Nuclei	<i>A</i>	<i>T</i> _{1/2}	<i>T</i> _{1/2} (GT+FF)	<i>T</i> _{1/2} (GT)	<i>T</i> _{1/2} (KHF)	<i>T</i> _{1/2} (QRPA-1)	<i>T</i> _{1/2} (QRPA-2)	<i>T</i> _{1/2} (GT)	<i>T</i> _{1/2} (GT+U1F)
Co	77	0.015	—	—	0.020	0.010	0.015	0.025	0.016
Ni	78	0.122	0.134	0.489	0.066	0.332	0.326	1.210	0.102
Cu	79	0.241	0.182	0.276	0.076	0.358	0.212	0.436	0.235
Zn	80	0.562	1.039	—	0.255	3.025	2.033	0.851	0.557
Ga	81	1.217	1.322	1.555	0.404	1.684	1.852	3.387	1.083

In Table V, the results of *β*-decay half-life calculations for waiting-point nuclei having *N* = 82 are shown. The calculations are compared with measured data [28] and previous computations. We have included the LSSM calculation [36] which includes both GT and FF contributions for these *N* = 82 isotones in the r-process domain. The FRDM+RPA calculation [31], considering only allowed GT results, is also shown. The last two columns depict our results. We note an excellent agreement of our calculated values with measured data once the U1F contribution is taken into account.

TABLE V

Comparison of our computed β -decay half-lives (in units of seconds) for $N = 82$ r-process waiting-point nuclei with previous calculations and experimental half-lives [28].

Nuclei	A	Exp.	Ref. [36]	Ref. [31]	Ref. [30]			This work	
		$T_{1/2}$	$T_{1/2}$ (GT+FF)	$T_{1/2}$ (GT)	$T_{1/2}$ (KHF)	$T_{1/2}$ (QRPA-1)	$T_{1/2}$ (QRPA-2)	$T_{1/2}$ (GT)	$T_{1/2}$ (GT+U1F)
Tc	125	0.008	—	0.009	—	—	—	0.017	0.008
Ru	126	0.017	—	0.034	—	—	—	0.027	0.017
Rh	127	0.028	—	0.022	—	—	—	0.032	0.029
Pd	128	0.035	—	0.125	—	—	—	0.042	0.035
Ag	129	0.050	0.035	0.047	0.084	0.033	0.033	0.052	0.049
Cd	130	0.127	0.146	1.123	0.138	0.655	0.655	0.135	0.122
In	131	0.261	0.177	0.147	0.216	0.146	0.146	0.286	0.281

It may be seen from Table III, Table IV and Table V that our calculated $T_{1/2}$ values are in very good agreement with the measured half-lives. Besides few $N = 82$ nuclei, the U1F contribution substantially lowers the calculated half-lives, specially for $N = 50$ cases. It is noted that the inclusion of U1F rates to allowed GT rates improves the comparison of our computed half-life results with the measured data. It is concluded from our study that the calculated β -decay half-lives may be further improved by integrating the rank 0 and 1 operator values to the forbidden transitions (non-unique contributions) which we plan to investigate in the near future.

The β -delayed neutron emission probabilities were also estimated by employing the QRPA [21, 30] and the shell model [22] approaches. Table VI compares our pn -QRPA calculated β -delayed neutron emission probabilities with previous calculations and experimental predictions. Noticeable differences between previous computations and our calculated probabilities are seen in Table VI.

The total GT strength and centroid (in β -decay direction) for the $N = 50$ and 82 waiting-point nuclei using our pn -QRPA model are shown in Table VII. The table reveals placement of GT centroid at higher excitation energies in daughter for the $N = 50$ nuclei. Only a large model space (up to 7 major shells) made this calculation in the present formalism possible. Shown also in Table VII is the comparison of our calculated Ikeda sum rule with the theoretical prediction (which is model-independent). It may be seen that the Ikeda sum rule is fulfilled for even-even cases. For odd- A cases, the compliance is within 1%. Our cut-off excitation energy was 35 MeV, and it is possible that some GT strength was located beyond 35 MeV in daughter and hence our calculated Ikeda sum rule was not fulfilled in 100%.

TABLE VI

Comparison between theoretical and experimental predictions of β -delayed neutron emission probability values for the selected waiting-point nuclei.

Nucl.	A	Exp. [30]	LSSM [22]	Ref. [21]		Ref. [30]			This work
		P_n	P_n	P_n (GT)	P_n (GT+FF)	P_n (KHF)	P_n (QRPA-1)	P_n (QRPA-2)	P_n (GT+UIF)
Co	77	—	77.2	—	—	52.8	39.3	78.1	65.8
Ni	78	—	79	51.4	51.0	10.8	40.7	55.7	16.3
Cu	79	55	88.6	64.8	63.4	21.8	33.7	27.9	50.5
Zn	80	1	14.1	3.8	4.2	0.7	10.9	10.0	0.10
Ga	81	12.1	13	14.5	17.1	3.8	6.7	7.0	40.2

TABLE VII

Statistical data of pn -QRPA calculated GT strength distributions.

Waiting-point nuclei			Gamow–Teller data		Ikeda sum rule	
Nuclei	Z	A	Centroid $B(\text{GT}-)$	$\sum B(\text{GT}-)$	Calculated	Theoretical
Fe	26	76	26.3	76.1	72.0	72
Co	27	77	26.9	72.3	68.9	69
Ni	28	78	27.5	70.3	66.0	66
Cu	29	79	28.2	65.9	62.7	63
Zn	30	80	29.0	61.7	60.0	60
Ga	31	81	29.5	59.3	56.6	57
Tc	43	125	20.0	120.3	116.7	117
Ru	44	126	21.1	125.6	114.0	114
Rh	45	127	21.9	113.6	110.6	111
Pd	46	128	22.7	117.3	108.0	108
Ag	47	129	23.2	106.6	104.3	105
Cd	48	130	24.0	110.4	102.0	102
In	49	131	25.0	100.2	98.9	99

Moving on from terrestrial to stellar environment, we investigate the electron emission (β^-) and (continuum) positron capture (e^+) rates for density range ($10\text{--}10^{11}$ g cm $^{-3}$) and temperature range ($0.01 \leq T_9 \leq 30$) for our selected thirteen r-process waiting-point nuclei. In order to save space, we decided to show results of one even–even and one odd- A nuclei for the $N = 50$ and 82 waiting-point cases. Figures 1–4 show the calculated weak rates for ^{77}Co , ^{80}Zn , ^{125}Tc and ^{130}Cd , respectively. Each figure consists of three panels. The upper panel shows the calculated sum of positron capture and electron emission rates in stellar environment as a function of core tem-

perature. It is to be noted that all parent excited states are contributing to the calculated (β^- and e^+) rate (see Eq. (16)). The middle panel depicts the calculated energy rates of β -delayed neutron in units of MeV s^{-1} . The bottom panel shows the calculated β -delayed neutron emission probabilities. Within the Q_β window, the β -delayed neutron emission probabilities (P_n) are required for the description of β strength functions and neutron separation energies. In all panels, we show the allowed GT and U1F contributions separately. All weak rates were calculated at a fixed stellar density of 10^6 g cm^{-3} (simulating an intermediate value of core density under stellar conditions).

For the intermediate density, the allowed rates in the upper panel of Fig. 1 are up to factor 2 bigger than the U1F rates at low stellar temperatures for ^{77}Co . It is further noted that with the increase of core temperature, the U1F rates increase at a faster pace and surpass the allowed rates, by up to a factor 8 at high T_9 values. At low core temperatures, more β -delayed neutrons are released due to U1F transitions than due to GT transitions. Accordingly, at low temperatures, the energy rates of β -delayed neutron, due to U1F transitions are by factor 3 bigger for ^{77}Co . The energy rates due to U1F transitions are more than an order of magnitude bigger at high stellar temperatures. The corresponding emission probabilities due to U1F

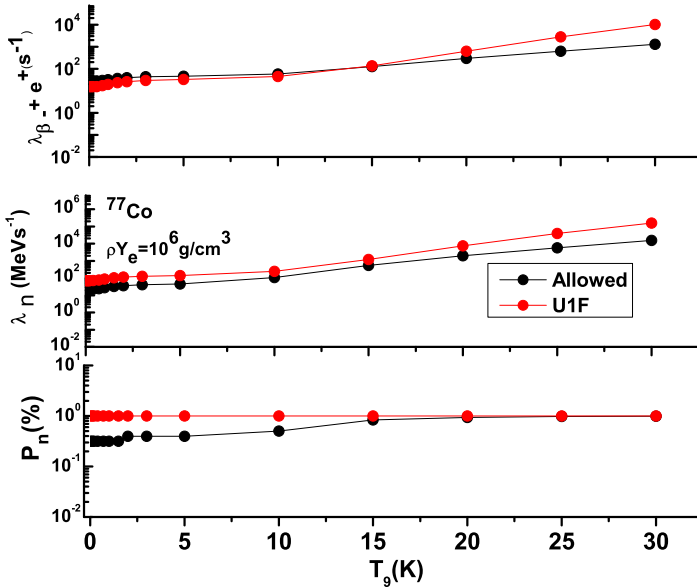


Fig. 1. The pn -QRPA calculated β^- decay and positron capture rates (upper panel), energy rates of β -delayed neutron (middle panel) and their emission probabilities (bottom panel) for ^{77}Co as a function of core temperature at stellar density of 10^6 g cm^{-3} . The allowed GT and U1F contributions are shown separately.

transitions are also appreciably greater as can be seen in the bottom panel of Fig. 1. At $T_9 = 30$ K, it is almost certain that β -delayed neutrons would be emitted, both due to allowed GT and U1F transitions. Similar trend was followed by other ($N = 50$) odd- A nuclei.

Figure 2 shows corresponding results for the waiting-point nuclei ^{80}Zn . Here, the allowed β -decay rates are by factor 3 bigger than the corresponding U1F rates at low temperatures. At $T_9 = 25$ K, the GT rates become comparable to U1F rates, while the U1F rates slightly surpass the GT rates at $T_9 = 30$ K. The energy rates due to GT transitions are comparable to U1F at low temperature. For the range of $T_9 = (0.7-5)$ K, the GT rates are up to a factor 2 bigger than U1F rates. The U1F rates slightly surpass the GT rates at $T_9 = 30$ K. Other $N = 50$ even-even nuclei followed a similar trend.

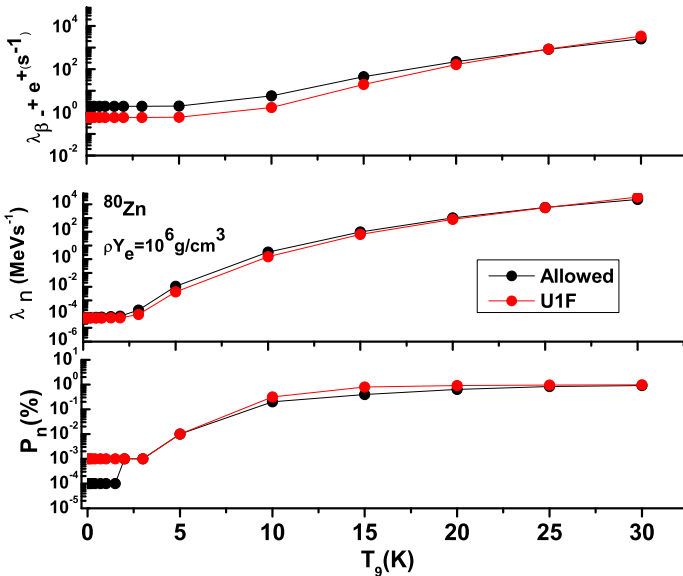


Fig. 2. The same as Fig. 1 but for ^{80}Zn .

Moving on to $N = 82$ waiting-point nuclei, Fig. 3 shows the pn -QRPA calculated weak rates for ^{125}Tc . Here, the U1F β -decay rates are bigger than GT rates up to factor 16 at $T_9 = 5$ K. The GT rates surpass the U1F rates at higher temperatures. The energy rates due to U1F transitions are more than an order of magnitude bigger at low temperatures. It is further noted that with the increase of core temperature, the energy rates due to allowed transition increase and surpass the U1F rates at high T_9 values. The corresponding emission probabilities due to GT transitions are also lower than U1F at low temperatures and surpass U1F at high core temperatures as can be seen in the bottom panel of Fig. 3.

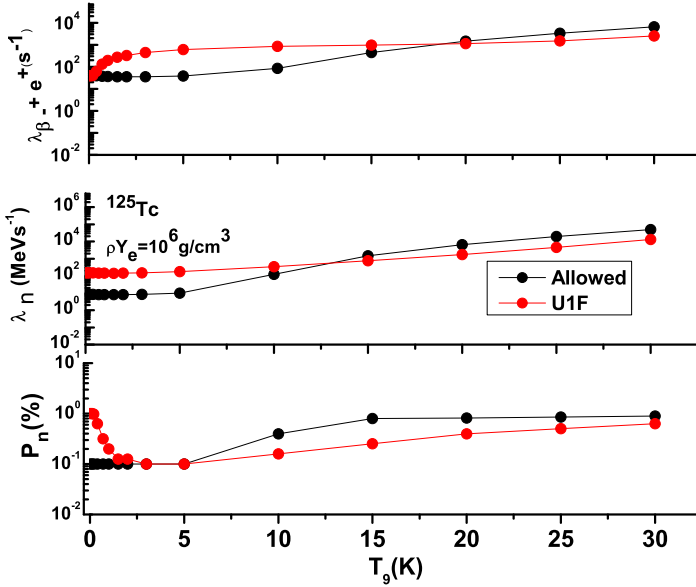


Fig. 3. The same as Fig. 1 but for ^{125}Tc .

The weak rate calculations for ^{130}Cd is presented in Fig. 4. The β -decay rates due to GT transitions are by factor 4 bigger than U1F transitions at low stellar temperatures, while at high temperatures, these rates are bigger

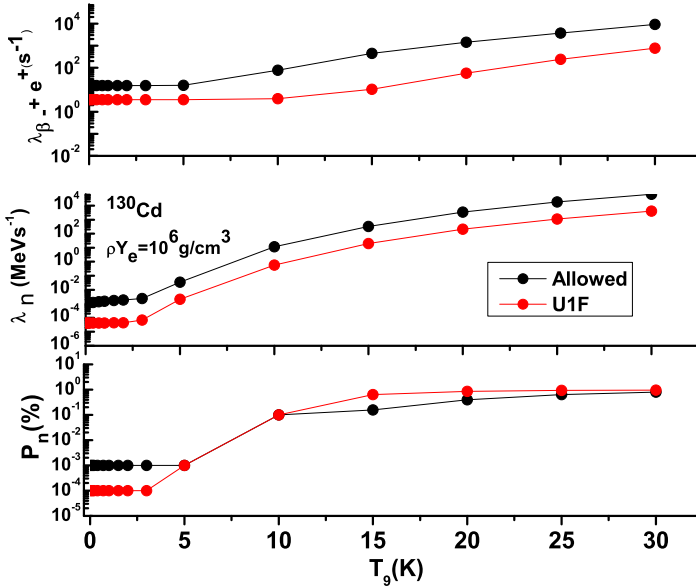


Fig. 4. The same as Fig. 1 but for ^{130}Cd .

than U1F up to a factor of 42 at $T_9 = 15$ K. The middle panel shows that the energy rates due to GT transitions are bigger than energy rates due to U1F transition on the average by a factor of 27.

At low stellar temperatures, positron capture rates may safely be neglected in comparison to β -decay rates. Only at high core temperatures ($kT > 1$ MeV), positron appears via $e^- - e^+$ pair creation. Positron capture rates become on a par with β -decay rates at $T_9 = 30$ K (in fact for ^{81}Ga , they are an order of magnitude bigger than β -decay rates). In general, the weak rates are product of phase space and reduced transition probabilities (directly linked with strength distribution functions). The reason for the behavior of pn -QRPA calculated weak rates depicted in Figs. 1-4 may be traced to the allowed and U1F strength distributions and phase-space calculations which we discuss next.

In Fig. 5 and Fig. 6, we show the phase-space calculation for allowed and U1F transitions as a function of core temperature for $N = 50$ and $N = 82$ waiting-point nuclei, respectively, at stellar density of 10^6 g cm^{-3} . We chose the same density at which we showed the calculation of weak rates earlier. The phase-space calculation for $N = 50$ nuclei in Fig. 5 displays certain distinctive features. At low stellar temperatures, the U1F phase space is bigger by as much as an order of magnitude compared to the allowed phase space. ^{81}Ga is an exception where the allowed phase space is bigger roughly by an order of magnitude at $T_9 = 0.01$ K. The phase space initially increases at a fast pace till the core temperature approaches $T_9 = 1$ K. Beyond this temperature, the phase space remains almost constant till $T_9 = 30$ K. At high temperatures, the two phase spaces are roughly the same for ^{76}Fe , ^{77}Co , ^{78}Ni and ^{79}Cu . Allowed phase space is bigger (smaller) than U1F phase space at high temperatures for ^{80}Zn (^{81}Ga).

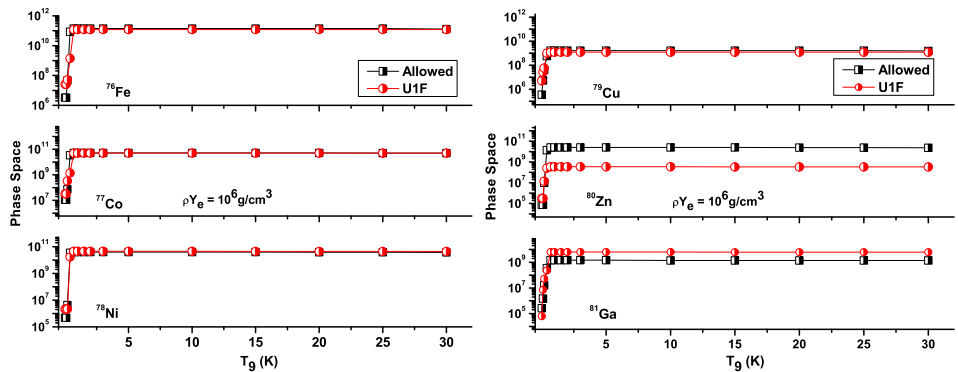


Fig. 5. Calculated phase space for allowed (GT) and unique first-forbidden (U1F) β -decay for $N = 50$ waiting-point nuclei for ^{76}Fe , ^{77}Co , ^{78}Ni , ^{79}Cu , ^{80}Zn and ^{81}Ga as a function of stellar temperature at selected density of 10^6 g cm^{-3} .

Figure 6 shows a few similarities of phase-space calculation for $N = 82$ waiting-point nuclei with the $N = 50$ case. Once again, the allowed phase space is orders of magnitude smaller than the U1F phase space at low temperatures (with the exception of ^{127}Rh). The rate of increase of phase space with temperature is rapid till $T_9 = 1$ K and almost none beyond this temperature. In all six cases, we note that the U1F phase space is bigger by as much as one order of magnitude at all temperatures (the only exception being ^{127}Rh at $T_9 = 0.01$ K). This is one reason why U1F transitions contribute significantly to the total weak rates for $N = 82$ waiting-point nuclei.

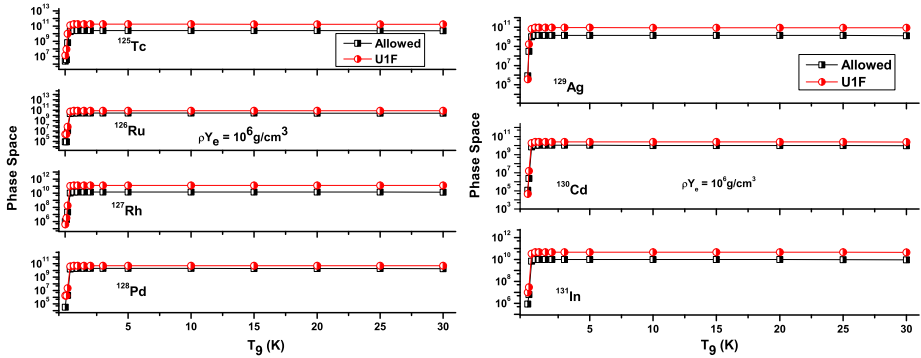


Fig. 6. The same as Fig. 5 but for $N = 82$ waiting-point nuclei for ^{125}Tc , ^{126}Ru , ^{127}Rh , ^{128}Pd , ^{129}Ag , ^{130}Cd and ^{131}In .

The skyscrapers for the calculated charge-changing strength distributions along β -decay direction for thirteen waiting-point nuclei are shown in Fig. 7 and Fig. 8. For each nucleus, the bottom panel shows the U1F transitions and the upper panel the allowed GT transitions, respectively. We note significant contribution from U1F transitions for $N = 50$ cases, while for $N = 82$ cases, the U1F contributions are relatively small. It is noted in Fig. 7 that U1F transitions are bigger in magnitude than the allowed GT transitions for ^{76}Fe , ^{78}Ni and ^{81}Ga . This is the reason that the terrestrial half-lives are reduced by $\sim 79\%$, $\sim 91\%$ and $\sim 68\%$ for ^{76}Fe , ^{78}Ni and ^{81}Ga , respectively, when U1F transitions were incorporated in pn -QRPA calculation (see Table III). The U1F transitions are relatively smaller in magnitude than the allowed GT transitions for the rest of $N = 50$ cases. Accordingly, the reduction in half-life values after incorporation of U1F transitions for these nuclei are smaller ($\sim 35\%$, $\sim 46\%$ and $\sim 34\%$ for ^{77}Co , ^{79}Cu and ^{80}Zn , respectively). The U1F contributions were relatively small for the $N = 82$ cases except for ^{125}Tc and ^{127}Rh (see Fig. 8). For ^{125}Tc , the U1F transitions were comparable in magnitude with the allowed GT transition and this is the reason the half-life is reduced by $\sim 50\%$ when U1F transi-

tion was incorporated (see Table III). For the case of ^{127}Rh , even though the U1F contribution is significant from Table III, it can be seen that the half-life is reduced only by 11%. The reason for this is traced back to the phase-space calculation where it is seen from Fig. 6 that at $T_9 = 0.01$ (at this low temperature, stellar phase space would be close to the terrestrial

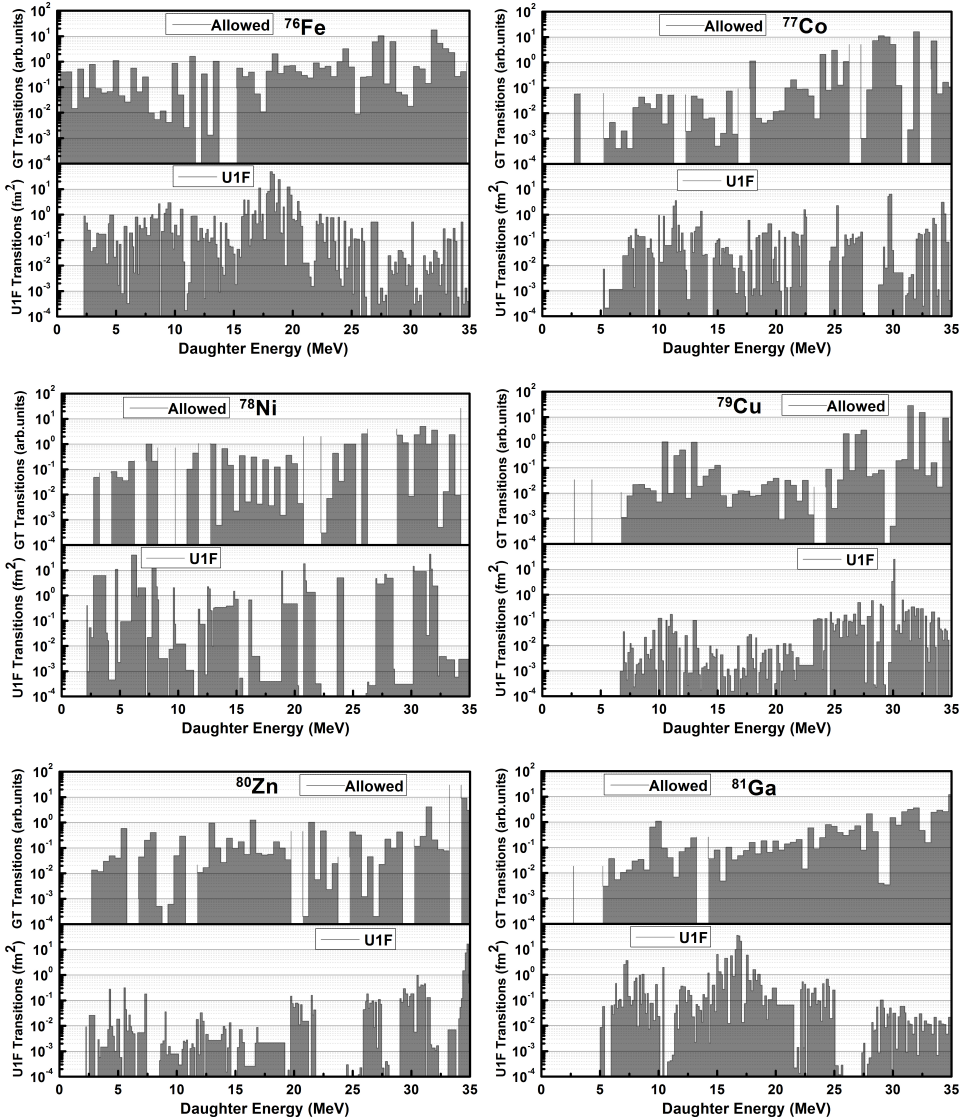


Fig. 7. Allowed and unique-first forbidden (U1F) β -decay transitions of $N = 50$ r-process waiting-point nuclei for ^{76}Fe , ^{77}Co , ^{78}Ni , ^{79}Cu , ^{80}Zn and ^{81}Ga as a function of daughter excitation energy calculated using the pn -QRPA model.

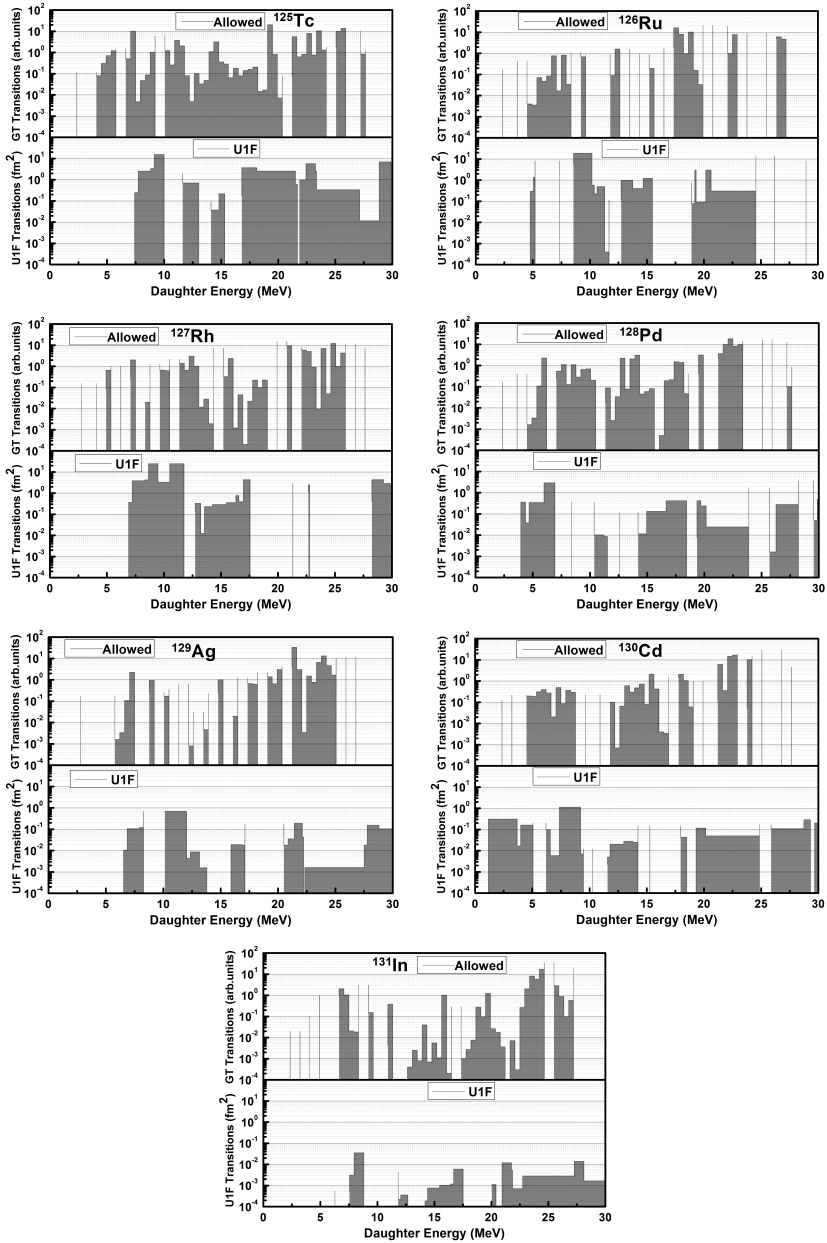


Fig. 8. Allowed and unique-first forbidden (U1F) β -decay transitions of $N = 82$ r-process waiting-point nuclei for ^{125}Tc , ^{126}Ru , ^{127}Rh , ^{128}Pd , ^{129}Ag , ^{130}Cd and ^{131}In as a function of daughter excitation energy calculated using the pn -QRPA model.

phase space), the U1F phase space is roughly an order of magnitude smaller than the allowed phase space. For the rest of the $N = 82$ cases, the U1F transition contributed up to $\sim 20\%$ in reducing the calculated terrestrial half-lives (see Table III).

4. Summary

For the first time, we present the allowed GT and U1F weak rates of $N = 50$ and $N = 82$ waiting-point nuclei in stellar environment using the deformed pn -QRPA model. The charge-changing strength distributions, phase-space and weak rate calculations, separately for allowed and U1F transitions, were calculated for a total of thirteen r-process waiting-point nuclei. Our results were compared with previous model calculations. The pn -QRPA calculation fulfilled the model-independent Ikeda sum rule, except for a few odd- A cases. The pn -QRPA calculated half-lives, after incorporation of U1F transitions, were in decent agreement with the measured half-lives and, at the same time, were also suggestive of incorporation of non-unique forbidden contributions which we plan to take as a future assignment. We found substantial U1F contribution to the β -decay half-lives for the $N = 50$ waiting points. It is hoped that the present study would prove useful for a better and reliable simulation of nucleosynthesis calculation.

The neutrino-driven wind streaming out of the neutron star forming at the center of a type II supernova has been shown to be one of possible candidates for the site of r-process. If r-process happened in a neutron-rich environment, then the electron neutrino capture could compete with the β -decay rates and is capable of modifying the r-abundance distribution by subsequent ν -induced neutron spallation. We plan to calculate the charged-current electron neutrino capture as a future assignment.

The weak rates for all thirteen waiting-point nuclei as a function of stellar temperature and density are available as ASCII files and may be requested from the corresponding author.

J.-U. Nabi would like to acknowledge the support of the Higher Education Commission Pakistan through project numbers 5557/KPK/NRPU/R&D/HEC/2016 and 9-5(Ph-1-MG-7)Pak-Turk/R&D/HEC/2017 and the Pakistan Science Foundation through project number PSF-TUBITAK/KP-GIKI (02).

REFERENCES

- [1] E.M. Burbidge, G.R. Burbidge, W.A. Fowler, F. Hoyle, *Rev. Mod. Phys.* **29**, 547 (1957).
- [2] R.H. Cyburt, B.D. Fields, K.A. Olive, T.H. Yeh, *Rev. Mod. Phys.* **88**, 015004 (2016).
- [3] K. Nomoto, C. Kobayashi, N. Tominaga, *Annu. Rev. Astron. Astrophys.* **51**, 457 (2013).
- [4] J.J. Cowan, F.-K. Thielemann, J.W. Truran, *Phys. Rep.* **208**, 267 (1991).
- [5] M. Arnould, K. Takahashi, *Rep. Prog. Phys.* **62**, 395 (1999).
- [6] K.-L. Kratz *et al.*, *Astrophys. J.* **403**, 216 (1993).
- [7] S.E. Woosley *et al.*, *Astrophys. J.* **433**, 229 (1994).
- [8] K.-L. Kratz *et al.*, *J. Phys. G* **24**, 331 (1988).
- [9] P.T. Hosmer, *Phys. Rev. Lett.* **94**, 112501 (2005).
- [10] K.-L. Kratz *et al.*, in: Proceedings of the International Conference on Fission and Properties of Neutron-Rich Nuclei, Sanibel Island, 1997, J.H. Hamilton (Ed.), World Scientific Press, Singapore, 1998.
- [11] K.-L. Kratz *et al.*, *Z. Physik A — Atomic Nuclei* **325**, 489 (1986).
- [12] B. Pfeiffer, K.-L. Kratz, F.-K. Thielemann, W.B. Walters, *Nucl. Phys. A* **693**, 282 (2001).
- [13] S. Nishimura, *Phys. Rev. Lett.* **106**, 052502 (2011).
- [14] T. Kurtukian-Nieto, *Nucl. Phys. A* **827**, 587C (2009).
- [15] H.V. Klapdor-Kleingrothaus, J. Metzinger, T. Oda, *At. Data Nucl. Data Tables* **31**, 81 (1984).
- [16] A. Staudt, E. Bender, K. Muto, H.V. Klapdor-Kleingrothaus, *Z. Physik. A — Atomic Nuclei* **334**, 47 (1989).
- [17] A. Staudt, E. Bender, K. Muto, H.V. Klapdor-Kleingrothaus, *At. Data Nucl. Data Tables* **44**, 79 (1990).
- [18] M. Hirsch, A. Staudt, K. Muto, H.V. Klapdor-Kleingrothaus, *At. Data Nucl. Data Tables* **53**, 165 (1993).
- [19] H. Homma *et al.*, *Phys. Rev. C* **54**, 2972 (1996).
- [20] P. Möller, B. Pfeiffer, K.-L. Kratz, *Phys. Rev. C* **67**, 055802 (2003).
- [21] I.N. Borzov, *Phys. Rev. C* **71**, 065801 (2005).
- [22] Q. Zhi *et al.*, *Phys. Rev. C* **87**, 025803 (2013).
- [23] J.-U. Nabi, H.V. Klapdor-Kleingrothaus, *Eur. Phys. J. A* **5**, 337 (1999).
- [24] J.-U. Nabi, H.V. Klapdor-Kleingrothaus, *At. Data Nucl. Data Tables* **71**, 149 (1999).
- [25] J.-U. Nabi, H.V. Klapdor-Kleingrothaus, *At. Data Nucl. Data Tables* **88**, 237 (2004).
- [26] N.B. Gove, M.J. Martin, *At. Data Nucl. Data Tables* **10**, 205 (1971).

- [27] P. Möller, J.R. Nix, W.D. Myers, W.J. Swiatecki, *At. Data Nucl. Data Tables* **59**, 185 (1995).
- [28] G. Audi *et al.*, *Chin. Phys. C* **41**, 030001 (2017).
- [29] J.-U. Nabi, N. Çakmak, Z. Iftikhar, *Eur. Phys. J. A* **52**, 1 (2016).
- [30] B. Pfeiffer, K.-L. Kratz, P. Möller, *Prog. Nucl. Energy* **41**, 39 (2002).
- [31] P. Möller, J.R. Nix, K.-L. Kratz, *At. Data Nucl. Data Tables* **66**, 131 (1997).
- [32] M. Majid, J.-U. Nabi, G. Daraz, *Astrophys. Space Sci.* **362**, 108 (2017).
- [33] K. Langanke, G. Martínez-Pinedo, *Rev. Mod. Phys.* **75**, 819 (2003).
- [34] J.J. Cuenca-García *et al.*, *Eur. Phys. J. A* **34**, 99 (2007).
- [35] P. Hosmer *et al.*, *Phys. Rev. C* **82**, 025806 (2010).
- [36] G. Martínez-Pinedo, K. Langanke, *Phys. Rev. Lett.* **83**, 4502 (1999).